

TEMPERATURE DEPENDENT ULTRASONIC PROPERTIES APPLIED TO A FINITE ELEMENT MODEL TO EVALUATE BIOLOGICAL TISSUES TEMPERATURE VARIATIONS

S.A. López-Haro^a, H. Calás^b, A. Ramos^c, A. Vera^a, L. Leija^a

^aCentro de Investigación y de Estudios Avanzados del Instituto Politécnico Nacional (Cinvestav –IPN)
Department of Electrical Engineering – Bioelectronics Section, Mexico D. F., Mexico.

^bConsejo Superior de Investigaciones Científicas, CSIC, Lab. Ultrasonic Signals, Systems and Technologies,
CAEND, Madrid, Spain

^cConsejo Superior de Investigaciones Científicas, CSIC, Lab. Ultrasonic Signals, Systems and Technologies,
Madrid, Spain

slopezh84@gmail.com; arvera@cinvestav.mx; lleija@cinvestav.mx

Abstract

The effects provoked by non-linear propagation, speed-of-sound (SOS) changes and sample thickness variations have been studied to evaluate changes in the transducer acoustic fields of high intensity focused ultrasound (HIFU) and, as a consequence, in the generated temperature distributions. Tissue thermodependent acoustic properties variations can produce hot-spots in not desired regions. In the SOS case, the transducer focus can suffer shifts forward or backward depending on the tissue composition. Some biological tissue temperature dependence of both the SOS and the attenuation of ultrasound has been measured in the temperature range from 25°C to 50°C; these thermodependent properties of fat, muscle, and liver are included in a finite element model to evaluate their effects in the acoustic field generated by an array of 4 concentric piezoelectric rings in a multilayer region. The radiated region is composed by 4 layers: skin, fat, muscle and liver. Temperature distributions provoked in the multilayer region were obtained after a simulated therapy of 5 s. There are differences of almost 4°C between temperature distributions of models with and without thermodependent properties. Absorption effects are more noticeable in the temperature distributions; SOS effects are minimal in acoustic fields. These effects must be taken into account to plan hyperthermia and ablation treatments in order to avoid hot-spots in not desired regions.

Keywords: Acoustic Fields, Attenuation, Finite Element Model, Speed-of-Sound, Temperature Distribution.

PACS no. 43.80.Cs; 43.80.Ev; 87.10.Kn;

1 Introduction

In recent years, the thermal therapy has emerged as a promising tool against cancer. This therapy can be classified with respect to the treatment temperatures; Stauffer [1] propose this classification from cryotherapy ($T < -50^{\circ}\text{C}$) to thermal ablation ($T > 50^{\circ}\text{C}$). The hyperthermia purpose is the cancer cell temperature elevation between 4°C and 8°C above its normal level to produce sensitization to both chemotherapy and radiotherapy [1]. Hyperthermia effects depend on applied energy, treatment time and biological tissues properties [2-4]. On the other hand, as mentioned above, thermal ablation occurs when the temperature reached is over 50°C ; the objective of this kind of procedures is to generate cancer cell necrosis being minimally invasive [5, 6] without surrounding tissues damage.

Thermal therapy can be applied by external, interstitial and intracavitary means [1]. One way to apply external thermal therapy is by using the High Intensity Focused Ultrasound (HIFU) [7, 8] which consists of the ultrasound energy focalization in a point by using both a transducer with a special geometry or a transducers arrangement [9]. This latter can be implemented by spatial configurations or by time delays.

Temperature distributions induced by HIFU transducers in biological tissues have been studied by several groups. Hynynen *et al.* studied the effect of the blood perfusion rate in the temperature distribution generated by a HIFU transducer in a dog kidney model proposing a multilayer geometry. Davies *et al.* used analytical models to obtain the acoustic field of a multi-transducer HIFU system. Later, Moros *et al.* compared *in vitro* and simulation results of temperature distributions achieved by a linear array of transducers in a perfused dog kidney. By other hand, numerical simulations have been used recently to evaluate the effects of non-linear propagation [10], refraction [11], sample thickness variations [11] and speed-of-sound (SOS) [11, 12] on the acoustic field of transducers and generated temperature distributions. Hallaj *et al.* use Bamber and Hill [13] results of SOS to study the thermo-acoustic lens effect in a model with a HIFU transducer and two layers of tissue; they found that the size and position of the focus is affected by the SOS variations.

The aim of this work is the evaluation of the effects of both the SOS and the attenuation of biological tissues in acoustic field and temperature distributions when the temperature dependence of the acoustic properties is added into a finite element (FE) model. Attenuation and SOS temperature dependence of *in vitro* pig liver, muscle and fat samples has been measured; obtained results were employed in a multilayered finite element (FE) model. The FE model was used to simulate the temperature elevation in biological tissues when they are heated by an arrangement of concentric piezoelectric rings focused by using time delays; bio-heat equation was employed to find the temperature distribution. Temperature distributions and acoustic fields with and without thermodependent properties are obtained and compared in the results section of this work.

2 Model Description

In this section, the conditions to solve the problem by using a FE model are presented; the model consists of an array of concentric piezoelectrics focalized at 10 mm, and 4 tissue layers to be heated: skin, fat, muscle and liver. The model was solved by using a work station Dell Precision T7400 with an Intel® Xeon® processor @ 3.00 GHz and 64.0 GB of RAM memory. The nature of the problem requires the combination and coupling of both the acoustic and the bioheat equations. The geometry

allows simplifying this problem into a 2D axisymmetric case, Figure 1. The processing time is reduced by this consideration and the solution is valid for the 3D case.

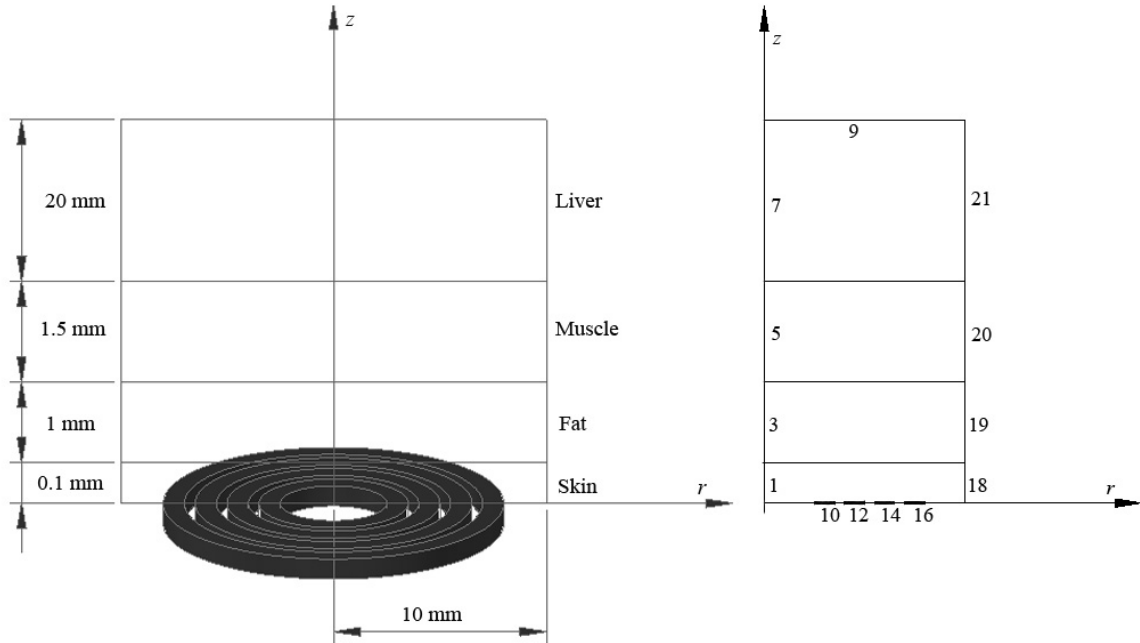


Figure 1 – Problem geometry consists of 4 tissue layers and an arrangement of concentric piezoelectric rings radiating the tissues (left). Simplification of the 3D geometry to a 2D axisymmetric case (right).

2.1 The Acoustic Model

The second-order hyperbolic partial differential equation that describes the wave propagation in a medium without losses is

$$\frac{1}{\rho} \nabla^2 p - \frac{1}{\rho c_s(T)^2} \frac{\partial^2 p}{\partial t^2} = q, \quad (1)$$

where ρ is the medium density, c_s is the media longitudinal speed-of-sound, q is an external source and p is the pressure. The SOS in biological tissues depends on water and fat content[14]; this behavior can accelerate or delay the wave propagation in the media. In a single circular transducer of radius r , the point where the Fresnel zone ends and Fraunhofer zone starts is determined by

$$z = \frac{r^2}{\lambda} = \frac{fr^2}{c_s(T)}. \quad (2)$$

The effects of the temperature variations in the transducer acoustic field can be observed if the SOS temperature dependence is added into the equations (1) and (2).

Because of the main objective of this work was the analysis of the effects of temperature dependent ultrasonic properties in the acoustic fields and as a consequence in the temperature distributions, the piezoelectric rings were simplified by using sinusoidal signals at 2 MHz in the boundaries 10, 12, 14, and 16. The pressure in the model was the sum of these 4 concentric rings contribution. The transducer excitation was performed so that the arrangement had a focus at 10 mm; focalization was achieved by using time delays in boundaries 12, 14 and 16. The excitation was carried out from the outermost rings to the inner. The acoustic field of the ring arrangement was obtained with and without temperature dependent properties.

2.2 The bioheat equation model

The temperature distribution generated in the tissue layers by the concentric ring arrangement were obtained by using the Pennes bioheat transfer equation [15]; this equation describes the behavior of the temperature increase in soft tissues by

$$\rho C \frac{\partial T}{\partial t} - k \nabla^2 T = \rho_b C_b \omega_b (T_b - T) + Q_{met} + Q_{ext} \quad (3)$$

where C and C_b are the heat capacities of tissue and blood, respectively; k is the thermal conductivity; ρ_b is the blood density; ω_b is the blood perfusion rate; T_b is the blood temperature; Q_{met} is the heat due to metabolism and Q_{ext} is the heat deposition due to an external source, acoustic pressure in this case.

The heat produced by the acoustic pressure depends on the acoustic intensity, I , and the tissue absorption coefficient, α ,

$$Q = 2\alpha I, \quad (4)$$

where the acoustic intensity and the pressure are related by

$$I = \frac{p^2}{2\rho c_s}. \quad (5)$$

If the metabolism effects are not considered, the bioheat and the acoustic equations can be coupled in the FE model solution by

$$\rho C \frac{\partial T}{\partial t} - k \nabla^2 T = \rho_b C_b \omega_b (T_b - T) + \frac{\alpha(T) p^2}{\rho c_s(T)}, \quad (6)$$

where the temperature dependence of both absorption coefficient and SOS can be considered.

The functions that describe the thermodependent behavior of absorption and SOS, as well as the densities and thermal properties [16-18] used in the model are summarized in the Table 1. Notice that in the model all attenuation was considered as a product of the tissue absorption.

Table 1 – Biological tissues thermal and acoustic properties. These properties were assigned to each subdomain in the FE model [16-18].

Tissue	SOS [m s ⁻¹]	Absorption at 2 MHz [Np m ⁻¹]	Density [kg m ⁻³]	Heat Capacity [J kg ⁻¹ K ⁻¹]	Thermal Conductivity [W m ⁻¹ K ⁻¹]
Skin	1540	0.4	1100	3598.2	0.209
Fat	-3.428T+1549	10.858-0.428T+0.0045T ²	918	3221.7	0.402
Muscle	1.558T+1546	3.059-0.099T+0.001T ²	1049	3807.0	0.618
Liver	0.8599T+1558	20.28-1.165T+0.0214T ²	1060	3500.0	0.498

*Temperature (T) is considered in °C.

2.3 FE model

Model grid was considered, according to literature [19-21], to have at least 6 elements per wavelength; this results in 8640 rectangular elements. Boundaries 1, 3, 5, and 7 were the axial axis of the problem. Taken into account that the geometry was drawn in cylindrical coordinates (r , z), the piezoelectric array was placed at $z=0$ and the skin, fat, muscle and liver layers were built from here. The peripheral boundaries (9, 18, 19, 20 and 21) had the same acoustic impedance of the corresponding tissue and the whole system was established as thermally isolated.

3 Results

Acoustic field of piezoelectric arrangement focused at 10 mm and temperature distributions generated were found in four cases: i) without the temperature dependence of SOS and absorption properties, values at 37°C were used; ii) only with the temperature dependence of SOS; iii) only with the temperature dependence of absorption, and iv) with the temperature dependence of both SOS and absorption.

3.1 Acoustic Field and Temperature Distribution

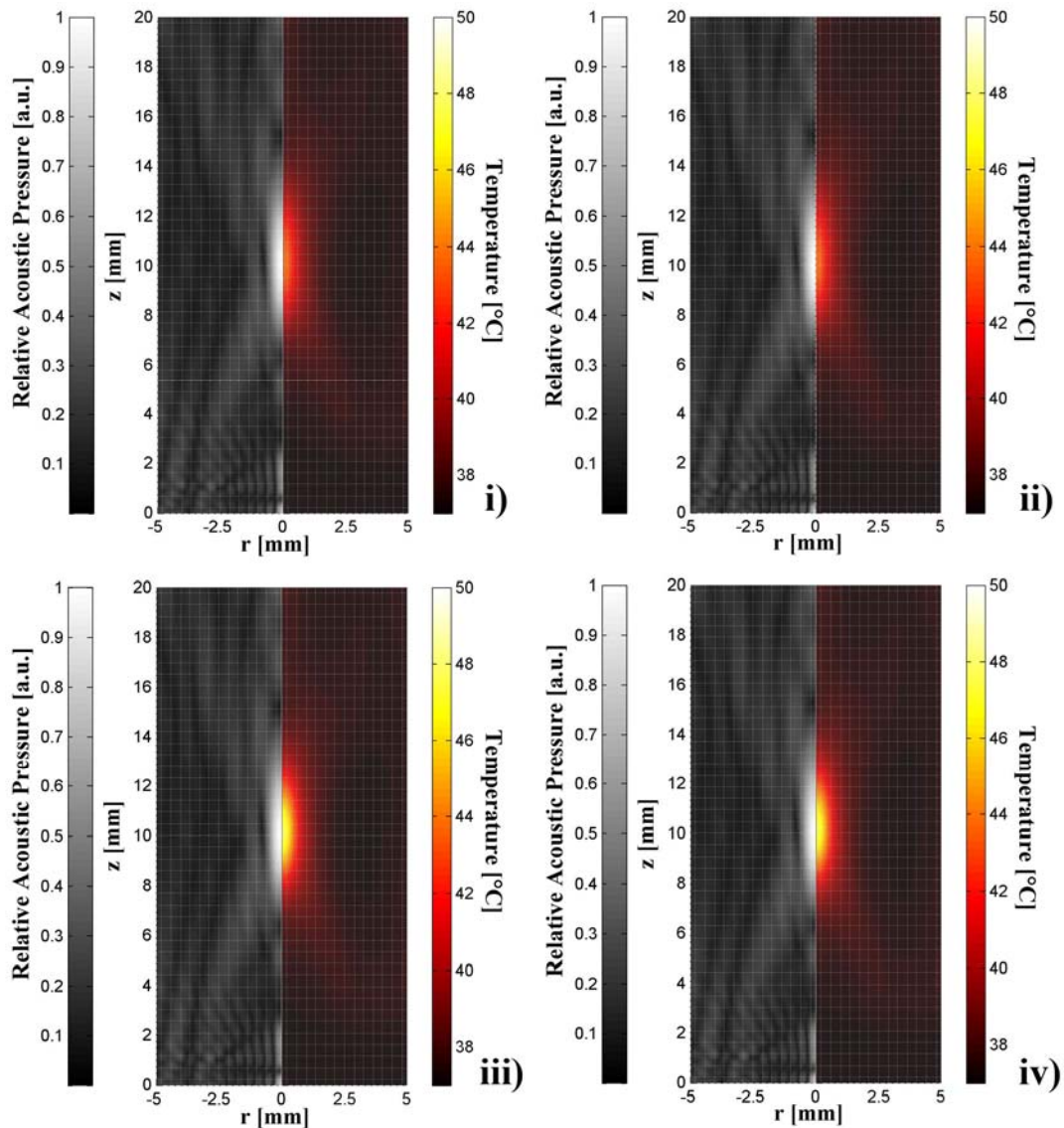


Figure 2 – Acoustic Field (left) and temperature distribution (right) achieved after 5 seconds of simulated therapy. Four cases are presented: i) SOS and absorption of ultrasound values at 37°C; ii) by using the temperature dependence of SOS; iii) by using the temperature dependence of absorption, and iv) by using the temperature dependence of both SOS and absorption.

Acoustic Field (left) and temperature distribution (right) achieved after 5 seconds of simulated therapy for the four cases mentioned above are shown in Figure 2. Acoustic field shows the focalization at 10 mm of the four piezoelectric rings for the four cases; acoustic pressure was normalized to compare qualitatively the focus shape in the central z axis. Temperature distributions were evaluated to obtain the maximum focal temperature achieved in each case, focus length and width, and the area with temperature above 43°C. Table 2 contains the results of the 4 cases analysis. Cases i) and ii) present no considerable differences between them, however, cases iii) and iv) have a difference of almost 4°C regarding the first two cases. Treatment area with temperature above 43°C is approximately 4.2 higher in the cases iii) and iv) than cases i) and ii).

Table 2 – Summary of maximum focal temperature, focus length and width, and the area with temperature above 43°C

	Maximum Focal Temperature [°C]	Length [mm]	Width [mm]	Area with T > 43°C [mm ²]
Case i)	43.734	1.88	0.46	0.679
Case ii)	43.683	1.86	0.46	0.672
Case iii)	47.696	3.54	1.03	2.864
Case iv)	47.517	3.54	1.029	2.861

3.2 Relative Acoustic Pressure and Temperature in the Transducer Central Axis

Evolution of the simulation is presented in Figure 3. Relative acoustic pressure (top) and temperature (bottom) in the central z axis of the simulation are presented every second from t = 0 s to t = 5 s. According with the relative acoustic pressure figures, focus localization suffers no significant variations at the end of the simulation when the temperature dependence of both SOS and absorption is added into the models. Temperature difference between cases with and without the absorption temperature dependence at t = 0 s is 0.6°C and at t = 5 s is 3.95°C.

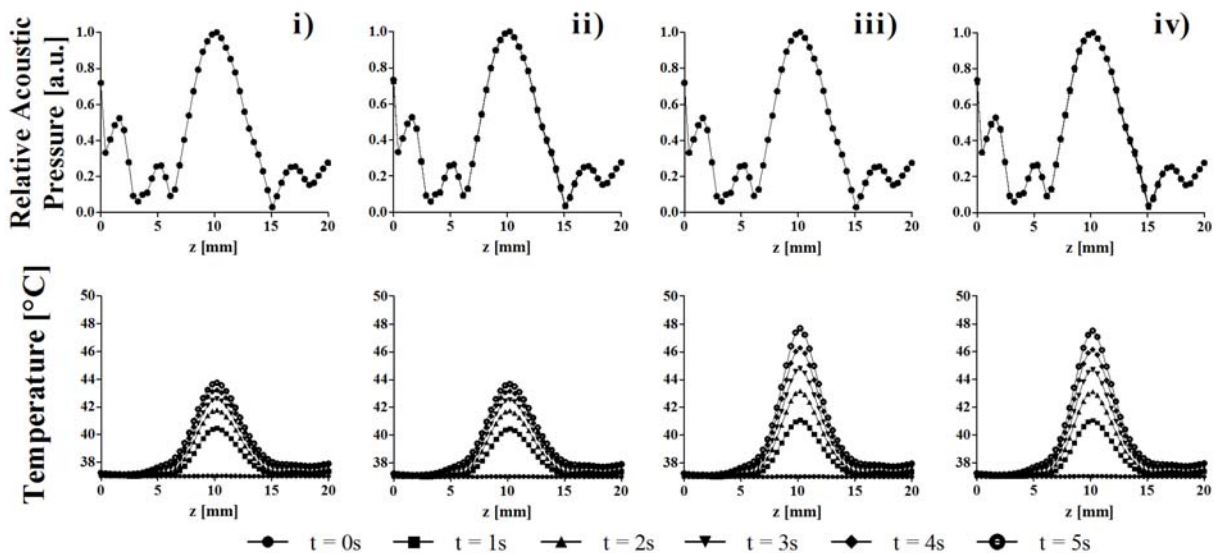


Figure 3 – Relative acoustic pressure (top) and temperature (bottom) evolution along central z axis for the four simulated cases.

4 Conclusions

SOS temperature dependence inclusion (cases ii and iv) decreases the final maximum temperature achieved at focus while effects of temperature dependent absorption (cases iii and iv) increase considerably the temperature at the end of the simulation. It is possible that the contribution of the SOS temperature dependence will be more noticeable in longer time simulation and when the achieved temperatures are higher. The employed linear functions to describe SOS variations can be replaced with quadratic functions and this can increase the effects of the SOS temperature dependence in both the acoustic field and the temperature distribution. Biological tissue acoustic characterization must be extended beyond 50°C because the temperature range used in the acoustic characterization limits the simulation process; we cannot assure that these functions are valid beyond 50°C. On the other hand, temperature dependence of thermal properties like heat capacity and thermal conductivity must be added in future models to have simulations closer to the reality. Finally, the effects produced by SOS and attenuation thermodependence must be taken into account to plan hyperthermia and ablation treatments in order to avoid hot-spots in not desired regions.

Acknowledgement

S.A. López-Haro acknowledges Conacyt Mexico for the fellowship 210059. This work was partially supported by the project M10-S02 of program ECOS-ANUIES-CONACYT and the ICyTDF project PICCO10-78.

References

- [1] P. R. Stauffer, "Evolving technology for thermal therapy of cancer," *Int J Hyperthermia*, vol. 21, pp. 731-44, Dec 2005.
- [2] W. D. O'Brien, Jr., C. X. Deng, G. R. Harris, B. A. Herman, C. R. Merritt, N. Sanghvi, and J. F. Zachary, "The risk of exposure to diagnostic ultrasound in postnatal subjects: thermal effects," *J Ultrasound Med*, vol. 27, pp. 517-35; quiz 537-40, Apr 2008.
- [3] A. Vera, J. E. C. Quero, L. Leija, Y. H. Mier, and C. Marchal, "Electromagnetic hyperthermia, an alternative to cancer treatment: history, physical and biological aspects. Hipertermia electromagnética, una alternativa para el tratamiento del cáncer: antecedentes, aspectos físicos y biológicos," *Revista Mexicana de Ingeniería Biomédica*, vol. XXII, pp. 78-88, 2001.
- [4] R. A. Steeves, "Hyperthermia in cancer therapy: where are we today and where are we going?," *Bull N Y Acad Med*, vol. 68, pp. 341-50, Mar-Apr 1992.
- [5] C. J. Diederich, "Thermal ablation and high-temperature thermal therapy: Overview of technology and clinical implementation," vol. 21, pp. 745-753, 2005.
- [6] P. R. Stauffer and S. N. Goldberg, "Introduction: Thermal ablation therapy," *Int J Hyperthermia*, vol. 20, pp. 671-677, 2004.
- [7] G. t. Haar and C. Coussios, "High Intensity Focused Ultrasound: Past, present and future," *International Journal of Hyperthermia*, vol. 23, pp. 85-87, 2007.
- [8] G. T. Haar and C. Coussios, "High intensity focused ultrasound: physical principles and devices," *Int J Hyperthermia*, vol. 23, pp. 89-104, Mar 2007.
- [9] B. L. Davies, S. Chauhan, and M. J. S. Lowe, "A Robotic Approach to HIFU Based Neurosurgery," in *Proceedings of the First International Conference on Medical Image Computing and Computer-Assisted Intervention*: Springer-Verlag, 1998.
- [10] F. P. Curra, P. D. Mourad, V. A. Khokhlova, R. O. Cleveland, and L. A. Crum, "Numerical simulations of heating patterns and tissue temperature response due to high-intensity focused

- ultrasound," *Ieee Transactions on Ultrasonics Ferroelectrics and Frequency Control*, vol. 47, pp. 1077-1089, Jul 2000.
- [11] D. H. Li, G. F. Shen, J. F. Bai, and Y. Z. Chen, "Focus Shift and Phase Correction in Soft Tissues During Focused Ultrasound Surgery," *Ieee Transactions on Biomedical Engineering*, vol. 58, pp. 1621-1628, Jun 2011.
- [12] I. M. Hallaj, R. O. Cleveland, and K. Hynynen, "Simulations of the thermo-acoustic lens effect during focused ultrasound surgery," *Journal of the Acoustical Society of America*, vol. 109, pp. 2245-2253, May 2001.
- [13] J. C. Bamber and C. R. Hill, "Ultrasonic attenuation and propagation speed in mammalian tissues as a function of temperature," *Ultrasound in Medicine & Biology*, vol. 5, pp. 149-157, 1979.
- [14] R. M. Arthur, W. L. Straube, J. W. Trobaugh, and E. G. Moros, "Non-invasive estimation of hyperthermia temperatures with ultrasound," *Int J Hyperthermia*, vol. 21, pp. 589-600, Sep 2005.
- [15] H. H. Pennes, "Analysis of tissue and arterial blood temperatures in the resting human forearm. 1948," *J Appl Physiol*, vol. 85, pp. 5-34, Jul 1998.
- [16] D. Haemmerich, I. d. Santos, D. J. Schutt, J. G. Webster, and D. M. Mahvi, "In vitro measurements of temperature-dependent specific heat of liver tissue," *Medical Engineering & Physics*, vol. 28, pp. 194-197, 2006.
- [17] K. R. Holmes, "Thermal Properties Appendix," <http://users.ece.utexas.edu/~valvano/research/Thermal.pdf>. Last accessed 11 July 2012.
- [18] A. R. Moritz, "Studies of Thermal Injury: III. The Pathology and Pathogenesis of Cutaneous Burns. An Experimental Study," *Am J Pathol*, vol. 23, pp. 915-41, Nov 1947.
- [19] N. N. Abboud, G. L. Wojcik, D. K. Vaughan, J. Mould, D. J. Powell, and L. Nikodym, "Finite element modeling for ultrasonic transducers," *Proc. SPIE Int. Symp. Medical Imaging*, pp. 19-42, 1998.
- [20] S. Jeyaraman and G. Baskaran, "Ultrasonic beam steering in isotropic media," in *COMSOL Users Conference*, Bangalore, 2006.
- [21] W. Ke and S. Chaki, "Finite element simulation of the critically refracted longitudinal wave in a solid medium," in *10ème Congrès Français d'Acoustique* Lyon, 2010.